Buckling analysis of explosive welded joints for ship structures

Pasqualino CORIGLIANO[a1], Vincenzo CRUPI[a], Eugenio GUGLIELMINO[a]
[a]*Department of Engineering, University of Messina.*

Abstract. Aluminum superstructures and steel hull connections are of fundamental importance in ships. This study regards the buckling analysis of explosion welded joints, made of three layers (ASTM A516 low carbon steel, pure aluminium, A5086 aluminium alloy) and used in ship structures. Experimental tests were carried out on explosion welded specimens. The Digital Image Correlation technique was applied during the tests for the detection of displacement and strain fields. A theoretical analysis, considering the different materials was also performed. Furthermore, a non-linear finite element analysis, considering the different mechanical properties of the explosive welded joint, was performed and was validated by means of the experimental results.

Keywords. Explosive welded joints, buckling, digital image correlation, non-linear finite element analysis, ship structures.

1. Introduction

Aluminium/steel welded joints are used in shipbuilding [1]. Generally, due to the difficulty of joining directly aluminium alloy to steel, an intermediate layer can be placed in between [2, 3]. The literature on the recent developments in explosive welding was reviewed in [4].

Experimental investigations of explosive welding of aluminium to steel were reported in literature [5, 6, 7].

The aim of this research activity was to study the non-linear behavior of aluminium/steel explosive welded joints used in shipbuilding, when they are subjected to compression loading and buckling takes place. The influence of the different materials was considered. The tensile properties of the materials were calculated from hardness measurements, according to the procedure reported in [8, 9], in order to perform a non-linear FE analysis, and the FE results were validated by means of the experimental data obtained through the Digital Image Correlation technique.

The authors have already applied full-field and non-destructive techniques (Infrared Thermography, Digital Image Correlation, Computed Tomography) for the analysis of different materials and welded joints used for marine structures: explosive welded joints under static and fatigue loadings [10], structural steel under static and fatigue loading [11, 12], and Iroko wood and laminates [13, 14].

[1] Pasqualino Corigliano, Corresponding author, Contrada di Dio - 98166 - Sant'Agata, Messina, Italy; E-mail: pcorigliano@unime.it.

2. Materials

The investigated explosive welded specimens, produced by TRICLAD, consist of ASTM A516 Gr55 structural steel, clad by explosion welding with AA5086 aluminum alloy and provided with an intermediate layer of AA1050 commercial pure aluminum. The heights of the layers are: 19 mm for the ASTM A516 Gr.55, 9.5 mm for the pure Aluminium 1050A, and 6 mm for the Aluminium alloy 5086; the thickness in the transversal direction is 3 mm. The measured hardness values for the three metals are: 175 HV for ASTM A516 gr 55, 47 HV for AA 1050 interlayer, 109 HV for AA 5086 [10]. With this kind of joints, it is not always possible to perform tensile tests on the virgin materials. Furthermore, the mechanical properties could be affected from the hardening due to the impact during the explosion welding process. For this reason, the non-linear properties were calculated from hardness measurements. The authors have reported in [10] the results of the yielding and ultimate stress as a function of the materials hardness. The obtained values are reported in table 1.

Table 1 . Obtained tensile properties from hardness measurements [10].

	Steel	**AA 5086**	**A 1050 A**
σ_Y [MPa]	380	285	90
σ_{ut} [MPa]	590	335	155

A method, which uses only the values of the ultimate and yielding stresses, was applied [15] in rder to obtain the treue stress-strain curves of the different materials. The method is based on the Ramberg-Osgood equation type:

$$\frac{E\varepsilon}{\sigma_Y} = \frac{\sigma}{\sigma_Y} + \alpha\left(\frac{\sigma}{\sigma_Y}\right)^m \tag{1}$$

Assuming the plastic strain at yielding $\varepsilon_{pY} = 0{,}002$, α and m are calculated as follows:

$$\alpha = \frac{E\varepsilon_{pY}}{\sigma_Y} \tag{2}$$

The relationship between m and the ultimate and yielding stresses, according to [15], was found equal to:

$$m = 3.93\left[\ln\left(\frac{\sigma_{ut}}{\sigma_Y}\right)\right]^{-0.754} \tag{3}$$

The values, obtained according to [15], are reported in table 2.

Table 2. R-O parameters determination according to [15].

	Steel	**AA 5086**	**A 1050 A**
σ_Y [MPa]	380	285	90
σ_{ut} [MPa]	590	335	155
m ($\varepsilon_{pY} = 0{,}002$)	7,30	15,53	6,20
α ($\varepsilon_{pY} = 0{,}002$)	1,08	0,50	1,57

The curves, obtained for the three materials using eq. (1), are shown in figure 2.

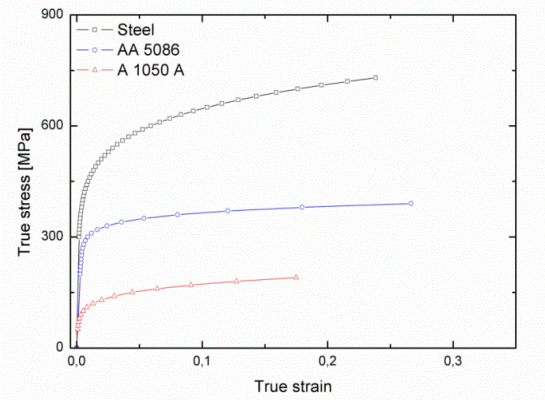

Figure 1. Ramberg-Osgood curves of the different materials.

3. Theoretical analysis

Buckling is defined as the tendency to deflect a beam if it is subjected to a certain compressive stress. In order for this phenomenon to occur, in reality it is necessary that the compression load is greater than the so-called critical load P_c[N]. To be able to calculate it usually makes reference to Euler's formula shown below:

$$P_c = \frac{\pi^2 E J_{min}}{l_0^2} \tag{4}$$

For a tri-material specimen, in the elastic phase, the stress will not be the same for each material but the strain will be the same, so the following relations can be assumed:

$$\sigma_1 = E_1\varepsilon\,; \qquad \sigma_2 = E_2\varepsilon\,; \qquad \sigma_3 = E_3\varepsilon\,; \tag{5}$$

Where subscripts 1, 2 and 3 refer to steel, pure aluminium and aluminium alloy respectively. Multiplying the stress by each area (width w and height h), the total force P can be expressed as:

$$\sigma_1 h_1 w + \sigma_2 h_2 w + \sigma_3 h_3 w = P \tag{6}$$

Which means:

$$E_1\varepsilon h_1 w + E_2\varepsilon h_2 w + E_3\varepsilon h_3 w = P \tag{7}$$

Obtaining that the axial strain is:

$$\varepsilon = \frac{P}{w\left(E_1 h_1 + E_2 h_2 + E_3 h_3\right)} \tag{8}$$

Allowing to evaluate the axial stresses as:

$$\sigma_1 = E_1 \frac{P}{w\left(E_1 h_1 + E_2 h_2 + E_3 h_3\right)} \tag{9}$$

$$\sigma_2 = E_2 \frac{P}{w\left(E_1 h_1 + E_2 h_2 + E_3 h_3\right)} \tag{10}$$

$$\sigma_3 = E_3 \frac{P}{w\left(E_1 h_1 + E_2 h_2 + E_3 h_3\right)} \tag{11}$$

From a theoretical point of view we can assume that when the three materials reach the critical stress, the whole specimen will undergo buckling phenomenon. The total critical load can be calculated as the sum of the critical load of each material.. Considering that the specimen is clamped from both ends ($l_0 = 0.5\ l$), the critical lad is:

$$P_{cth} = \frac{4\pi^2 E_1 J_{1min}}{l^2} + \frac{4\pi^2 E_2 J_{2min}}{l^2} + \frac{4\pi^2 E_3 J_{3min}}{l^2}$$

$$P_{cth} = 4\pi^2 \frac{\left(E_1 J_{1min} + E_2 J_{2min} + E_3 J_{3min}\right)}{l^2} \tag{12}$$

The total critical load and the critical stress of aluminium are plotted vs the specimen length in figure 2. Considering that the producer declared, for the aluminium,

a value of σ_y equal to 35 MPa, if a safety factor of 2 is applied, in order to have buckling before yielding, a value of 350 mm of the free length is obtained. Considering a length l= 350 mm and that the specimen is clamped from both ends the following values reported in table 3 are obtained:

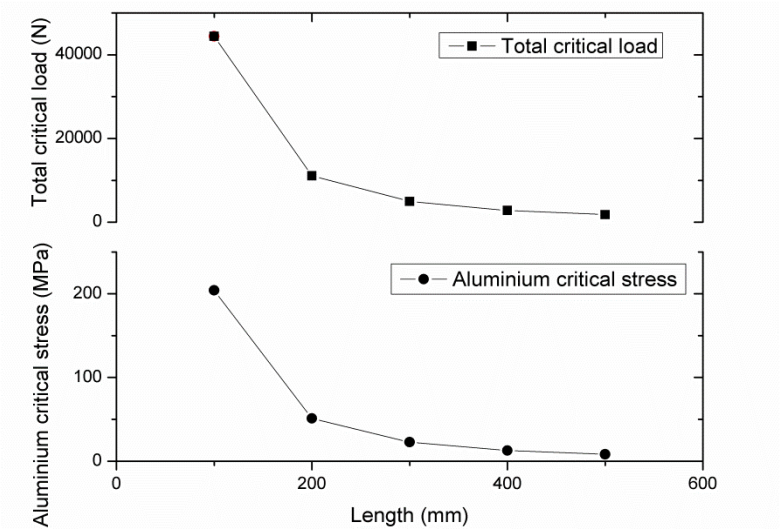

Figure 2. Total critical load and critical stress of aluminium vs specimen length.

Table 3. Critical load and stress calculated for each material and total critical load for all the welded joint.

P_{c1th} (N)	P_{c2th} (N)	P_{c3th} (N)	σ_{c1th} (MPa)	σ_{c2th} (MPa)	σ_{c3th} (MPa)	P_{cth} (N)
2852	475	300	50	16	16	3627

4. Experimental test

The tests were performed using an ITALSIGMA servo-hydraulic load machine with a 12 kN capacity. The tests were performed at a loading rate of 41,6 N/s. The ARAMIS 3D 12M system was used for the Digital Image Correlation analysis in order to detect full-field displacements and strains of the external surface of the specimen. The total length of the specimen could not be monitored otherwise a loss of accuracy in detecting the displacements would occur, so the two cameras were placed in correspondence of the middle length of the specimen, as shown in the experimental setup of figure 3, and the monitored length of each image was 150 mm. The specimens were coated with a black/white speckle pattern for the strain measurements. The specimen was clamped from both ends and the length between the grips was set to 350 mm. The experimental

setup is reported in figure 3, while figure 4 shows the evolution of the transverse displacement (out of plane displacement) of the external surface at different loads. It is easy to see that at the beginning of the test, the external surface of the specimen, lays on the origin of the coordinate axis (left side of figure 4) with very small values of transverse displacement: When buckling takes place, the specimen tends to deflect, (i.e. at 3200 N the specimen surface does not lay on the coordinate axis) and the transverse displacement increases with a loss of the load (bending is predominant in the right side of figure 4).

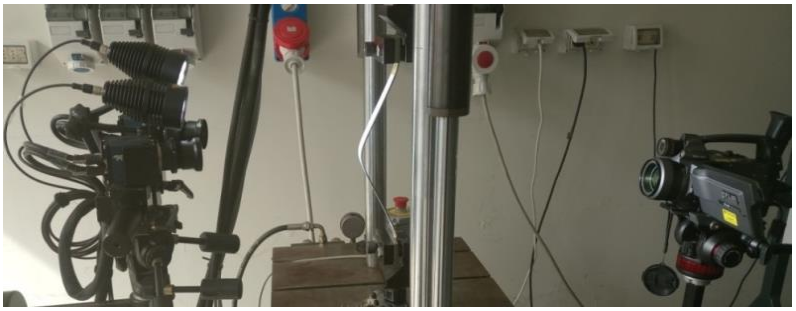

Figure 3. Experimental setup.

.

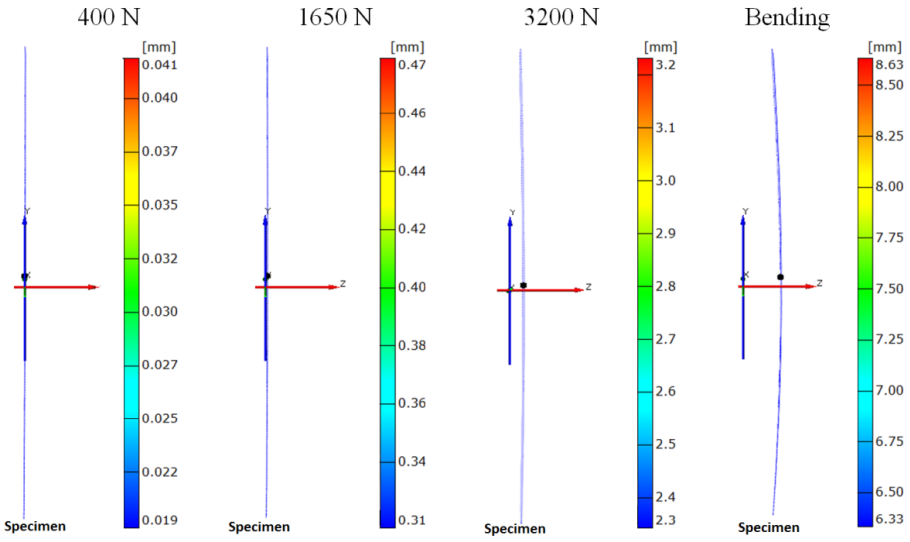

Figure 4. Transverse displacement (out of plane displacement) evolution at different loads.

This behaviour is further confirmed by figures 5 and 6 which plot he load versus the vertical and transverse displacements curves respectively. It has to be noted that buckling phenomenon, considering the transverse displacement measured by the DIC technique, starts to occur before the maximum registered load due to the deviation from linearity of the curve.

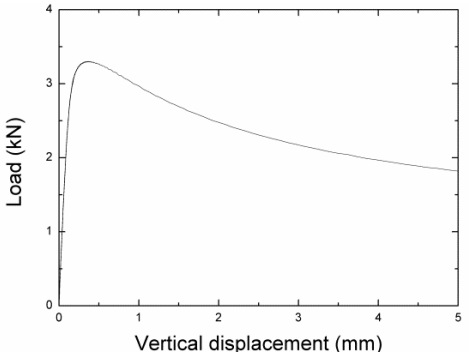

Figure 5. Load-vertical displacement curve.

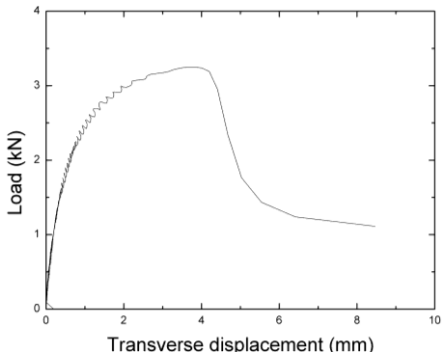

Figure 6. Load-transverse displacement curve.

5. Finite element analysis

The buckling analysis can be performed using the eigenvalue method; with this type of analysis is possible to predict the theoretical deformation strength of an ideal elastic structure. It allows calculating the structural eigenvalues for a given load. Obviously, in the actual conditions, the structural imperfections and the non-linearity of the material are such that the result obtained could not coincide with the real one.

Nonlinear buckling analysis is generally more accurate than eigenvalue analysis because it employs non-linear effects, large-deflection, etc, to predict buckling loads. Furthermore the non-linear material properties of the different materials (see figure 2) were considered in this study. The chosen element for the FE analyses was the solid186, having 20 nodes and three degrees of freedom: translation along the x, y and z directions; this element supports plasticity, iperplasticity, creep and large deflections in addition to having the ability to allow to simulate deformations of elastoplastic materials.

5.1. Finite element eigenvalues analysis

As regards the analysis of eigenvalues for a given load, a distributed load is applied at one end of the sample. This load was applied to generate a compressive stress, and with a unitary module in order to determine the critical load. The useful length of the specimen does not correspond to the total length of the same; in fact, the specimen is clamped at both ends by the grips, each of which has a length of 25 mm. This means that the length l is equal to 350 mm.

Figure 7 shows the results of the displaced specimen and the predicted value of the P_{cFE} which is 3637 N, being in good agreement with the calculated theoretical value (P_{cth} = 3627 N) and a little different than the experimental test results ($P_{cexp} \approx$ 3260 N).

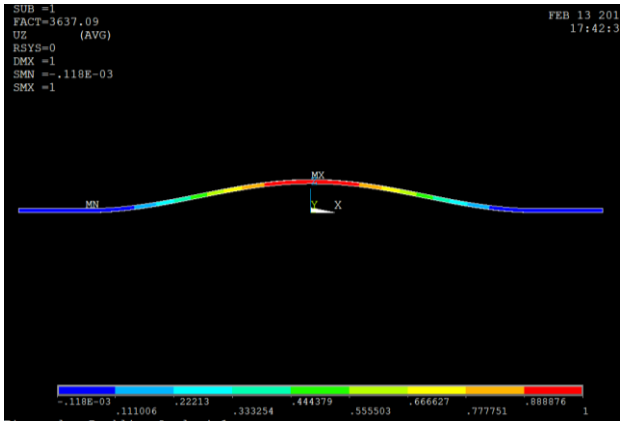

Figure 7. Results of the displaced specimen and predicted value of the P_{cFE}.

5.2 Nonlinear finite element analysis

The true non-linear nature of this analysis permits the modeling of geometric imperfections, load perturbations, material nonlinearities. For this type of analysis, small off-axis loads are necessary to initiate the desired buckling mode. The applied load is gradually increased until a load level is found whereby the structure becomes unstable; a very small increase in the load will cause suddenly very large deflections. Non-linear 3D FEA analyses were carried out using a gradual increase of the applied load. The mechanical properties of each material, detected from hardness measurements and previously reported in figure 2, were considered as input of the FE model using the Ansys software. Multi-linear kinematic hardening models were used in this study for the non-linear analyses. The transverse (out plane) displacement map at the maximum load is reported in figure 8.

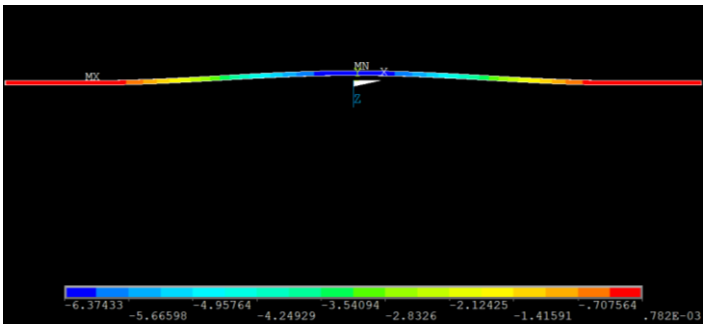

Figure 8. Transverse (out plane) displacement at the maximum load.

The non-linear FE analysis does not give a value of the critical load but, as the experimental test, is able to give the history of the test without the load loss, for this reason a comparison between the non-linear FEA and the experimental test is reported in figure 9, being in good agreement and confirming that the choice of calculating the

non-linear material properties, used for the non-linear FEA, from hardness measurements, leads to reliable results.

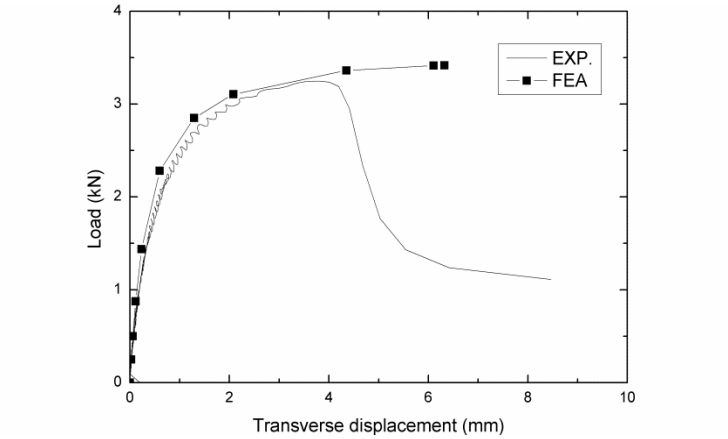

Figure 9. Non-linear FEA and experimental load-transverse displacement curve.

Furthermore figure 10 illustrates a comparison of the transverse displacement at 3200 N, reporting that both, FE and DIC results show that the Al alloy side has a bigger displacement.

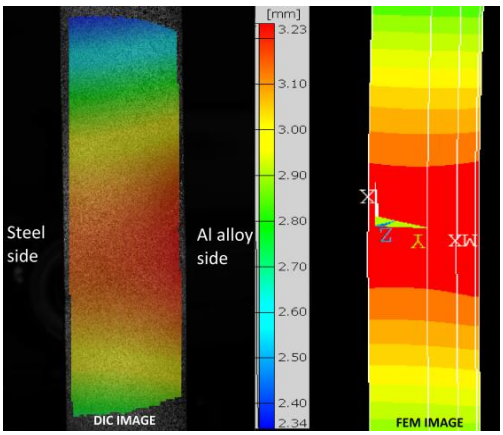

Figure 10. Transverse displacement at 3200 N: DIC and FE images.

Conclusion

The linear FE buckling analysis was in good agreement with the theoretical values but both give an overestimation of the critical load. Experimental tests showed that the buckling phenomenon, considering the transverse displacement measured by the DIC technique, starts to occur before the maximum registered load, due to the deviation from linearity of the curve. The non-linear FE analysis permits the modeling of

geometric imperfections, load perturbations, and material nonlinearities, and was in good agreement with the experimental investigation. Furthermore non-linear FE and DIC results show that, as expected, the Al alloy side has a bigger displacement.

Acknowledgements

The research reported in this paper was conducted with the facilities of the Research Project "CERISI" ("Research and Innovation Centre of Excellence for Structure and Infrastructure of large dimensions"), funded by the PON (National Operative Programme) 2007-2013. This study is part of the research activities of the Research Project PRIN (Announcement 2015) "CLEBJOINT", project funded by the Italian Ministry of Scientific and Technological Research.

References

[1] G.A. Young, J.G. Banker, Explosion welded, bi-metallic solutions to dissimilar metal joining. 13th Offshore Symposium (2004), Texas Section of the Society of Naval Architects and Marine Engineers, Houston, Texas.

[2] J.H. Han, J.P. Ahn, M.C Shin, Effect of interlayer thickness on shear deformation behaviour of AA5083 aluminium alloy/SS41 steel plates manufactured by explosive welding, *J. Mater. Sci.* (2003), 38:13.

[3] X. Li, H. Ma, Z. Shen, Research on explosive welding of aluminum alloy to steel with dovetail grooves. *Mater. Des.* **87** (2015), 815–824.

[4] F. Findik, Recent developments in explosive welding, *Mater. Des.* **32** (2011), 1081–1093.

[5] C.R. McKenney, J. Banker, Explosion – bonded metals for marine structural applications; *Marine Technology. Society of Naval Architects and Marine Engineers* (1971), 285-292.

[6] M. Acarer, B. Demir, An investigation of mechanical and metallurgical properties of explosive welded aluminium–dual phase steel, *Mater. Lett.* **62** (2008), 4158. .

[7] R. Chao, J. Yang, S. Lay, Interfacial toughness for the shipboard aluminum/steel structural transition joint, *Mar. Struct.* **10** (1997), 353-362

[8] Z. Lopez, A. Fatemi, A method of predicting cyclic stress-strain curve from tensile properties for steels. *Mat. Sci. Eng. A-Struct.* **556** (2012), 540–550.

[9] P.A. Stathers, A.K. Hellier, R.P. Harrison, M.I. Ripley, J. Norrish, Hardness-tensile property relationships for HAZ in 6061-T651 aluminum, *Weld. J.* **93** (2014), 301-311.

[10] P. Corigliano, V. Crupi,E. Guglielmino, A.M. Sili, Full-field analysis of AL/FE explosive welded joints for shipbuilding applications, *Mar. Struct.* **57** (2018), 207-218.

[11] P. Corigliano, V. Crupi, G. Epasto, E. Guglielmino, G. Risitano, Fatigue assessment by thermal analysis during tensile tests on steel, *Procedia Eng.* **109** (2015), 210–218.

[12] P. Corigliano, G. Epasto, E. Guglielmino, G. Risitano, Fatigue analysis of marine welded joints by means of DIC and IR images during static and fatigue tests, *Eng. Fract. Mech.* **183** (2017), 26–38.

[13] V. Bucci, P. Corigliano,V. Crupi, G. Epasto, E. Guglielmino, A. Marinò, Experimental investigation on Iroko wood used in shipbuilding, P. I. Mech. Eng. C-J. Mec **231** (2017), 128–139.

[14] P. Corigliano, V. Crupi, G. Epasto, E. Guglielmino, N. Maugeri, A. Marinò, Experimental and theoretical analyses of Iroko wood laminates, *Compos. Pt. B - Eng.* **112** (2017), 251–264.

[15] M. Kamaya, Ramberg–Osgood type stress–strain curve estimation using yield and ultimate strengths for failure assessments, *Int. J. Press. Vessel. Pip.* **137** (2016), 1–12.